

## 2D $\pi$ -conjugated benzo[1,2-*b*:4,5-*b'*]dithiophene- and quinoxaline-based copolymers for photovoltaic applications†

Cite this: *RSC Adv.*, 2013, **3**, 24543

Margherita Bolognesi,<sup>\*a</sup> Desta Gedefaw,<sup>\*b</sup> Dongfeng Dang,<sup>b</sup> Patrik Henriksson,<sup>b</sup> Wenliu Zhuang,<sup>b</sup> Marta Tessarolo,<sup>c</sup> Ergang Wang,<sup>b</sup> Michele Muccini,<sup>c</sup> Mirko Seri<sup>d</sup> and Mats R. Andersson<sup>\*b</sup>

Two medium gap semiconducting polymers, **P(1)-Q-BDT-4TR** and **P(2)-FQ-BDT-4TR**, based on alternate units of alkyl-dithiophene substituted benzodithiophene (BDT) and quinoxaline units (without or with fluorine substitution), are synthesized and fully characterized. The polymers exhibit optical and electrical properties favorable for being employed as donors in BHJ OPV devices, such as: absorption spectra extending up to around 720 nm for a high solar spectrum coverage, deep lying HOMO energy levels for a high device open circuit voltage and LUMO energy levels higher than those of PC<sub>61</sub>BM and PC<sub>71</sub>BM for an efficient exciton dissociation. In particular, the presence of alkyl-dithiophene side chains allows us to obtain a high 2D  $\pi$ -conjugation which promotes red shifted absorption profiles, low HOMO energy levels (<−5.6 eV) and enhanced environmental and thermal stability. Moreover, the introduction of the fluorine atom in the polymer backbone allows us to obtain efficient OPV devices, based on as-cast **P(2)-FQ-BDT-4TR**:PC<sub>61</sub>BM blend, showing a  $J_{SC}$  of −10.2 mA cm<sup>−2</sup>,  $V_{OC}$  of 0.90 V, FF of 58% and PCE of 5.3%, without the need for any additional thermal treatment.

Received 7th August 2013

Accepted 9th October 2013

DOI: 10.1039/c3ra44238a

[www.rsc.org/advances](http://www.rsc.org/advances)

### Introduction

Solution-processed organic solar cells (OPVs) represent the newest generation of technologies in solar power generation, offering benefits in terms of low manufacturing costs (*i.e.* high-throughput roll-to-roll processing), large area coverage, compatibility with flexible and light-weight substrates, earth-abundant constituents and architectural tunability over multiple length scales.<sup>1</sup> During the last decade, the power conversion efficiency (PCE) of these devices has increased dramatically due to the development of new materials,<sup>2</sup> engineered interfaces,<sup>3</sup> enhanced understanding of polymeric film microstructure and photophysics<sup>4</sup> and optimization of the devices architecture.<sup>5</sup> The highest OPV performance to date has been obtained for so-called bulk-heterojunction (BHJ) cell

architectures where the photoactive layer is composed of an interpenetrating network of bicontinuous electron-donor polymer (D) and electron-acceptor fullerene (A) domains, placed between a semitransparent anode (ITO, indium tin oxide) and a metal cathode.<sup>6</sup> Despite the impressive achievements in power conversion efficiency (PCE), there is still much room for the improvement of the performance of BHJ solar cells.<sup>7</sup> In particular, the properties of photoactive materials are one of the most determining factors on the overall performance of a polymer solar cell.<sup>8</sup> An ideal donor polymer should fulfill some fundamental requirements such as: broad absorption spectrum with high absorption coefficient, high charge carrier mobility and optimal energetic alignment of the HOMO and LUMO energy levels with those of the acceptor material (PC<sub>61</sub>BM or PC<sub>71</sub>BM) to ideally provide large open-circuit voltages ( $V_{OC}$ ),<sup>9</sup> increased environmental stability<sup>10</sup> and efficient exciton dissociation at the D–A interface.<sup>11</sup> Through a rational materials development, a wide variety of  $\pi$ -conjugated donor polymers, with desirable chemical and physical properties, were prepared and employed as efficient donor materials for BHJ solar cells.<sup>12</sup> Among these, the *push–pull* polymers, based on the combination of alternated electron-rich (*push*) and electron-deficient (*pull*) moieties, have attracted much attention due to their intrinsic advantages and potentials in optoelectronic devices.<sup>14,13</sup> This particular structure allows to effectively tune the energy of the HOMO–LUMO levels, the band gap and thus the light absorption properties of

<sup>a</sup>Laboratory MIST E-R, Via P. Gobetti, 101, 40129, Bologna, Italy. E-mail: m.bolognesi@bo.ismnr.cnr.it; Tel: +39 051 6399173

<sup>b</sup>Polymer Chemistry, Department of Chemical and Biological Engineering, Chalmers University of Technology, SE-412 96, Göteborg, Sweden. E-mail: antenehe@chalmers.se; mats.andersson@chalmers.se; Tel: +46 031 7723410; +46 031 7723401

<sup>c</sup>Consiglio Nazionale delle Ricerche (CNR), Istituto per lo Studio dei Materiali Nanostrutturati (ISMN), Via P. Gobetti, 101, 40129, Bologna, Italy

<sup>d</sup>Consiglio Nazionale delle Ricerche (CNR), Istituto per la Sintesi Organica e la Fotoreattività (ISOF), Via P. Gobetti, 101, 40129, Bologna, Italy

† Electronic supplementary information (ESI) available: Square wave voltammetry, NMR spectra, hole mobility measurements. See DOI: 10.1039/c3ra44238a

alternating polymers.<sup>14</sup> Moreover, recent studies demonstrate that such *push-pull* structures can promote charge carrier mobility due to the reduced interchain  $\pi$ - $\pi$  stacking distance.<sup>15</sup>

The wide possibility of combinations of comonomers in *push-pull* structures results in a wide variety of polymers with very different physical-chemical and optoelectronic properties.<sup>16</sup> Among these, it has been recently demonstrated the use of *push-pull* alternating copolymers based on quinoxaline and benzo[1,2-*b*:4,5-*b'*]dithiophene (BDT) moieties as highly efficient donor materials for BHJ solar cells.<sup>17</sup> The quinoxaline unit, usually sandwiched between adjacent thiophene spacers to limit the inter-monomers steric hindrance, is a strong electron acceptor unit widely used as building block for optoelectronic applications, since it can be easily modified and side-substituted to finely tune the optoelectronic properties of the resulting polymer.<sup>18</sup> On the other hand, BDT has been widely used as electron-rich co-monomer thanks to its desirable peculiarities such as structural rigidity and planarity leading to extended  $\pi$ -conjugation length and favorable inter-chain  $\pi$ - $\pi$  stacking, other than the presence of additional substitution sites for the incorporation of side chains.

The side substitution of the  $\pi$ -conjugated co-monomers is indeed an essential and widely spread technique used to modulate the chemical-physical properties of semiconducting polymers.<sup>19</sup> For instance, the introduction of strong electron withdrawing halogen atoms (*e.g.* fluorine)<sup>20</sup> on the polymer backbone allows to tune its electronic properties such as HOMO and LUMO energy levels and bandgap. In addition, it is known that the introduction of fluorine atoms increases the polymer charge carrier mobility by promoting stronger inter-chain interactions.<sup>21</sup> On the other hand, the use of alkyl substituted aromatic side groups on the copolymer backbone has been demonstrated to both enhance the solubility of the copolymer and contribute to extend the  $\pi$ -conjugation from the backbone to the lateral substituents, leading to two-dimensional or 2D  $\pi$ -conjugated systems.<sup>22</sup> Thiophene-based  $\pi$ -conjugated side chains, with the high electronic density and strong tendency to aggregation of this group, are particularly suitable for the described purposes. For example, Li *et al.*<sup>22a</sup> reported the synthesis and study of a 2D-conjugated polymer with alkylthiophene  $\pi$ -conjugated side chains, which showed red-shifted absorption spectrum, improved thermal stability, lower HOMO energy, significantly higher hole mobility and overall enhanced photovoltaic properties (PCEs up to 6%), in comparison with the corresponding alkoxy-substituted copolymer. Moreover, by further extending the  $\pi$ -conjugation of the side chain from a single thiophene unit to two or more, the described 2D-effects could be further enhanced.

Based on these considerations, we study here the effect of introducing conjugated side-chains (alkyl-dithiophenes) on quinoxaline – BDT based co-polymers by evaluating their optical, electronic, morphological and photovoltaic properties and comparing them to analogous polymers with similar backbone structures (same *push-pull* units) and unconjugated alkyl side chains. In particular we report the synthesis and characterization of two p-type copolymers **P(1)-Q-BDT-4TR** and **P(2)-FQ-BDT-4TR** (Fig. 1), where the BDT monomer, substituted with alkyl-

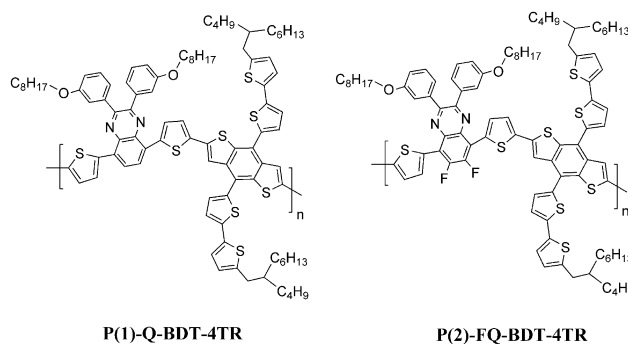


Fig. 1 Structure of **P(1)-Q-BDT-4TR** and **P(2)-FQ-BDT-4TR**.

dithiophene side groups to form a 2D-conjugated unit, is combined with an unsubstituted or fluorinated quinoxaline moiety (Q and FQ, respectively) sandwiched between two thiophene rings. The functionalization of the BDT core with electron-rich thiophene based side chains (4TR) is applied in order to obtain a broader absorption, a higher hole mobility and a lower HOMO energy level of the resulting polymer. The synergic effect of the  $\pi$ -conjugated side chains and fluorine atom substitution effectively allows to obtain a polymer with a strongly red shifted absorption maxima ( $\Delta\lambda_{\max} > 30$  nm) and a lowered HOMO level ( $\Delta E_{\text{HOMO}} > 0.1$  eV), with respect to the analogous polymer (PBBDT-TFQ)<sup>17b</sup> containing alkoxy side chains on the BDT unit. As a result, an OPV device with a  $J_{\text{SC}} = -10.5$  mA cm<sup>-2</sup>,  $V_{\text{OC}} = 0.90$  V and PCE = 5.5% has been fabricated.

## Experimental

### General

5,8-Dibromo-6,7-difluoro-2,3-bis(3-(octyloxy)phenyl)quinoxaline and 5,8-bis(5-bromothiophen-2-yl)-2,3-bis(3-(octyloxy)phenyl)quinoxaline were prepared according to previously reported procedures.<sup>18b,23</sup> Tetrahydrofuran (THF) was dried over Na/benzophenone and freshly distilled prior to use. Other reagents and solvents were commercial grade and used as received without further purification.

<sup>1</sup>H NMR and <sup>13</sup>C NMR spectra were acquired from a Varian Inova 400 MHz NMR spectrometer. Tetramethylsilane was used as an internal reference with deuterated chloroform as solvent. Size exclusion chromatography (SEC) was performed on Waters Alliance GPCV2000 with refractive index detector columns: Waters Styragel® HT 6E ×1, Waters Styragel® HMW 6E ×2. The eluent was 1,2,4-trichlorobenzene. The working temperature was 135°C and the resolution time was 2 h. The samples, with concentration of 0.5 mg mL<sup>-1</sup>, were filtered (filter: 0.45 μm) prior to the analysis. The molecular weights were calculated through calibration with polystyrene standards.

Square-wave voltammetry (SWV) measurements were carried out on a CH-Instruments 650A Electrochemical Workstation. A three-electrode setup was used with platinum wires both as working electrode and counter electrode, and Ag/Ag<sup>+</sup> used as reference electrode calibrated with Fc/Fc<sup>+</sup>. A 0.1 M solution of tetrabutylammonium hexafluorophosphate (Bu<sub>4</sub>NPF<sub>6</sub>) in anhydrous acetonitrile was used as supporting electrolyte. The

polymers were deposited onto the working electrode from chloroform solution. In order to remove oxygen from the electrolyte, the system was bubbled with nitrogen prior to each experiment. The nitrogen inlet was then moved to above the liquid surface and left there during the scans. HOMO and LUMO levels were estimated from the peak potentials of the third scan by setting the oxidative peak potential of Fc/Fc<sup>+</sup> vs. the normal hydrogen electrode (NHE) to 0.63 V (ref. 24) and the NHE vs. the vacuum level to 4.5 V.<sup>25</sup>

### Synthesis of monomers and polymers

**Synthesis of 6,7-difluoro-2,3-bis(3-(octyloxy)phenyl)-5,8-di(thiophen-2-yl)quinoxaline (2).** 5,8-Dibromo-6,7-difluoro-2,3-bis(3-(octyloxy)phenyl)quinoxaline (1) (1.3 g, 1.775 mmol), Pd<sub>2</sub>(dba)<sub>3</sub> (38 mg, 2.3 mol%), P(*o*-tolyl)<sub>3</sub> (45 mg, 6.3 mol%) were dissolved in THF (35 mL) and heated to reflux. 2-(Tributyl stannyl) thiophene (1.66 g, 1.41 mL, 4.44 mmol) was added drop by drop to the refluxing reaction mixture and heating continued for two days. The reaction mixture was cooled and THF was removed by rotary evaporator. To the remaining crude greenish material, hexane was added and a solid crushed out from the solution. The solid formed was separated by suction filtration and recrystallized from isopropanol and yielded 2 (0.8 g, 62%).

<sup>1</sup>H NMR (400 MHz, CDCl<sub>3</sub>, δ): 8.05 (1H, d, *J* = 4 Hz), 7.62 (1H, d, *J* = 4 Hz), 7.36 (1H, s), 7.26 (4H, m), 6.95 (1H, m), 3.92 (2H, t), 1.76 (2H, m), 1.43 (10H, m), 0.90 (3H, t).

<sup>13</sup>C NMR (100 MHz, CDCl<sub>3</sub>, δ): 159.01, 139.23, 130.80, 130.74, 129.90, 129.19, 126.60, 126.58, 122.73, 116.59, 115.61, 109.99, 68.12, 31.83, 29.33, 29.99, 29.13, 26.05, 22.68.

**Synthesis of 5,8-bis(5-bromothiophen-2-yl)-6,7-difluoro-2,3-bis(3-(octyloxy)phenyl)quinoxaline (3).** Compound 2 (0.8 g, 1.08 mmol) was dissolved in THF (40 mL) and NBS (0.38 g, 2.16 mmol) was added and stirred at room temperature for 3 hours after protecting the reaction from light by covering with aluminum foil. The mixture was poured on water and the orange solid formed was collected by filtration. The solid was recrystallized twice from isopropanol and the fluffy orange solid obtained was the desired product (0.5 g, 52%).

<sup>1</sup>H NMR (400 MHz, CDCl<sub>3</sub>, δ): 7.77 (1H, d, *J* = 4 Hz), 7.51 (1H, s), 7.23 (1H, t, *J* = 8 Hz), 7.16 (1H, d, *J* = 4 Hz), 7.08 (1H, d, *J* = 8 Hz), 7.00 (1H, dd, *J* = 4 Hz, 8 Hz), 4.05 (2H, t), 1.82 (2H, m), 1.51 (10H, m), 0.91 (3H, t).

<sup>13</sup>C NMR (100 MHz, CDCl<sub>3</sub>, δ): 159.38, 151.62, 138.71, 132.37, 130.86, 129.34, 129.08, 122.90, 118.88, 117.29, 115.09, 68.30, 31.85, 29.42, 29.32, 29.30, 26.17, 22.69, 14.13.

**Synthesis of 4,8-bis(5'-(2-butyloctyl)-[2,2'-bithiophen]-5-yl)-benzo[1,2-*b*:4,5-*b'*]dithiophene (5).** 5-(2-Butyloctyl)-2,2'-bithiophene (4) (2.27 g, 6.796 mmol) was dissolved in THF (35 mL) and cooled with an ice bath and stirred under nitrogen atmosphere. *n*-BuLi, 2.5 M (2.72 mL, 6.796 mmol) was added drop-by-drop to the reaction mixture over 18 minutes. The mixture was stirred for 1 hour and 45 minutes in the ice bath and then at ambient temperature for 30 minutes. The reaction mixture was heated at 50 °C for 1 hour and 15 minutes afterwards. Benzo[1,2-*b*:4,5-*b'*]dithiophene-4,8-dione (0.43 g, 1.95 mmol) was added and heated at 50 °C for 1 hour. The reaction mixture was cooled to

room temperature and SnCl<sub>2</sub>·2H<sub>2</sub>O (3 g, 13.3 mmol) dissolved in 10% HCl (7 mL) was added gradually and stirred at room temperature overnight. The reaction mixture was poured on water and extracted with diethyl ether. The ether extract was dried with anhydrous sodium sulfate and the solvent was removed to give a crude product. It was purified with silica gel column chromatography using hexane–chloroform (15 : 1) as eluent which yielded compound 5 (1.29 g, 77.3%).

<sup>1</sup>H NMR (400 MHz, CDCl<sub>3</sub>, δ): 7.69 (1H, d, *J* = 4 Hz), 7.50 (1H, d, *J* = 8 Hz), 7.38 (1H, d, *J* = 4 Hz), 7.24 (1H, d, *J* = 4 Hz), 7.09 (1H, d, *J* = 4 Hz), 6.70 (1H, d, *J* = 4 Hz), 2.77 (2H, d, *J* = 8 Hz), 1.68 (1H, m), 1.35 (16H, m), 0.97 (6H, m).

<sup>13</sup>C NMR (100 MHz, CDCl<sub>3</sub>, δ): 144.45, 139.06, 139.05, 137.61, 136.55, 134.56, 128.83, 127.82, 125.97, 123.62, 123.57, 123.27, 123.11, 39.99, 34.59, 33.18, 32.86, 31.90, 29.64, 28.86, 26.59, 23.02, 22.69, 14.16, 14.13.

**Synthesis of (4,8-bis(5'-(2-butyloctyl)-[2,2'-bithiophen]-5-yl)-benzo[1,2-*b*:4,5-*b'*]dithiophene-2,6-diyl)bis(trimethylstannane) (6).** Compound 5 (1.15 g, 1.34 mmol) was dissolved in THF (45 mL) and stirred in an ice bath for 1 hour. *n*-BuLi, 2.5 M (1.29 mL, 3.216 mmol) was added drop-by-drop with a syringe over 10 minutes. The reaction mixture was stirred in the bath for 1 hour and 20 minutes. The bath was removed and stirred for 1 hour and 30 minutes. Trimethyl tin chloride (4.02 mL, 4.02 mmol) was added in one portion and stirred overnight. The reaction mixture was poured on water and extracted with diethyl ether. The ether extract was washed with distilled water. The ether solution was dried with anhydrous sodium sulfate and solvent removed to yield a crude product which was purified by recrystallization from isopropanol two times. The solid was dried to give compound 6 (1.13 g, 71.1%).

<sup>1</sup>H NMR (400 MHz, CDCl<sub>3</sub>, δ): 7.70 (1H, s), 7.39 (1H, d, *J* = 4 Hz), 7.25 (1H, d, *J* = 4 Hz), 7.10 (1H, d, *J* = 4 Hz), 6.70 (1H, d, *J* = 4 Hz), 2.77 (2H, d, *J* = 8 Hz), 1.66 (1H, m), 1.32 (16H, m), 0.91 (6H, m), 0.41 (9H, s).

<sup>13</sup>C NMR (100 MHz, CDCl<sub>3</sub>, δ): 144.26, 143.35, 142.91, 138.74, 138.44, 137.38, 134.77, 130.89, 128.71, 125.93, 123.53, 123.13, 121.88, 39.99, 34.59, 33.18, 32.87, 31.90, 29.65, 28.86, 26.60, 23.03, 22.69, 14.17, 14.13, -8.27.

**Synthesis of P(1)-Q-BDT-4TR.** Compound 6 (0.137 g, 0.116 mmol) and 5,8-bis(5-bromothiophen-2-yl)-2,3-bis(3-(octyloxy)phenyl)quinoxaline (7) (0.1 g, 0.116 mmol) were dissolved in toluene (10 mL) and deaerated for 10 minutes. Pd<sub>2</sub>(dba)<sub>3</sub> (2.55 mg, 2.79 × 10<sup>-3</sup> mmol) and P(*o*-Tolyl)<sub>3</sub> (4.24 mg, 0.014 mmol) were added and the mixture was purged with nitrogen gas for 25 minutes. The reaction mixture was heated at 90 °C for 7 hours under nitrogen atmosphere. The polymer was end capped by adding tributyl(thiophen-2-yl)stannane (0.1 mL, 0.348 mmol) and 2-bromothiophene (0.09 mL, 0.92 mmol) and heating for more than 5 hours after the addition of each of the end capping reagents. The polymer solution was then added to methanol and the solid formed was collected by filtration. The polymer was re-dissolved in chloroform and 10% aqueous solution of sodium diethyldithiocarbamate trihydrate (100 mL) was added. The mixture was heated at 60 °C for 1 hour and 30 minutes followed by stirring at room temperature overnight. The chloroform soluble portion was separated and washed with distilled

water three times. The chloroform solution was reduced to small volume and then added to methanol. The solid formed was collected by filtration and then purified by Soxhlet extraction using methanol, hexane and diethyl ether. Finally, the polymer remaining in the thimble was extracted with chloroform. After reducing to small volume, the solution was precipitated by adding on methanol. The solid was collected by filtration, dried in vacuum oven at 40 °C overnight and yielded **P(1)-Q-BDT-4TR** as a brown solid (140 mg, 78%).

<sup>1</sup>H NMR (400 MHz, CDCl<sub>3</sub>, δ): 7.5–6.5 (aromatic protons), 4.0–3.5 (–OCH<sub>2</sub>–), 3.0–2.5 (–CH<sub>2</sub> adjacent to thiophene), 2.0–0.5 (other aliphatic protons).

**Synthesis of P(2)-FQ-BDT-4TR.** Compound **6** (0.11 g, 0.093 mmol) and compound **3** (0.0835 g, 0.093 mmol) were dissolved in toluene (5 mL) and deaerated with N<sub>2</sub> gas for 10 minutes. Pd<sub>2</sub>(dba)<sub>3</sub> (2.55 mg, 2.79 × 10<sup>−3</sup> mmol) and P(*o*-Tolyl)<sub>3</sub> (4.24 mg, 0.014 mmol) were added and purged with nitrogen gas for 25 minutes. The reaction mixture was heated at 90 °C for 1 hour and 20 minutes under nitrogen atmosphere. The polymer solution was then precipitated by adding on methanol. The solid formed was collected by filtration. The polymer was re-dissolved in chloroform by heating at 60 °C for 1 hour and a 10% aqueous solution of sodium diethyldithiocarbamate trihydrate (100 mL) was added and stirred overnight at room temperature. The chloroform soluble portion was separated and washed with distilled water three times. The chloroform solution was reduced to small volume and then added to methanol. The solid was collected by filtration and then purified by Soxhlet extraction using methanol, hexane, diethylether and dichloromethane. Finally, chloroform was used to wash out what was left in the thimble. The volume of the chloroform solution was reduced and the polymer was precipitated by adding on methanol. The solid was filtered and dried in vacuum oven at 40 °C to yield **P(2)-FQ-BDT-4TR** as a brown solid (96 mg, 65%).

<sup>1</sup>H NMR (400 MHz, CDCl<sub>3</sub>, δ): 7.5–6.5 (aromatic protons), 4.0–3.5 (–OCH<sub>2</sub>–), 3.0–2.5 (–CH<sub>2</sub> adjacent to thiophene), 2.0–0.5 (other aliphatic protons).

### OPV devices fabrication and characterization

Patterned ITO-coated glasses ( $R_s \sim 10 \Omega \text{ sq}^{-1}$ ) were cleaned in sequential sonicating baths (for 15 min) in deionized water, acetone and isopropanol. After the final sonication step, substrates were dried with a stream of N<sub>2</sub> gas and then placed in an oxygen plasma chamber for 10 min. Next, a thin layer (~30 nm) of PEDOT:PSS (Clevios P VP Al 4083) was spun-cast on the ITO surface and subsequently annealed at 150 °C for 15 min. The samples were then transferred inside the glove box (<0.1 ppm of O<sub>2</sub> and H<sub>2</sub>O) for active layer and top contact deposition. In the meantime, the active layer blend solutions were formulated inside the glove box. For optimized devices, a total polymer-fullerene concentration of 30 mg mL<sup>−1</sup> in *o*-dichlorobenzene was used for both polymers. The mixture solutions were stirred overnight at 80 °C and then spun-cast on top of the ITO/PEDOT:PSS surface. Before cathode deposition, the substrates were then either thermally annealed or left as-cast. To complete the device fabrication, LiF/Al cathode (0.6 nm/100 nm) were next

deposited sequentially without breaking vacuum ( $\sim 3 \times 10^{-6}$  Torr) using a thermal evaporator directly connected to the glove box. The current–voltage (*I*–*V*) characteristics of complete OPV devices were recorded by a Keithley 236 source-measure unit under simulated AM1.5 G illumination of 100 mW cm<sup>−2</sup> (Abet Technologies Sun 2000 Solar Simulator). The light intensity was determined by a calibrated silicon solar cell fitted with a KG5 color glass filter to bring spectral mismatch to unity. The active area of the solar cell was exactly 6 mm<sup>2</sup>. During testing, each cell was carefully masked, by calibrated mask, to prevent an excess photocurrent generated from the parasitic device regions outside the overlapped electrode area. All solar cells were tested inside the glove box with oxygen and moisture free environment.

External Quantum Efficiency (EQE) was measured with a home built system on encapsulated devices: monochromatic light was obtained with a Xenon arc lamp from Lot-Oriel (300 Watt power) coupled with a Spectra-Pro monochromator. The photocurrent produced by the device passed through a calibrated resistance (50 Ω) and the voltage drop signal was collected through the resistance with a Lock-In Digital Amplifier-SR830. Signal was pulsed by means of an optical chopper (~500 Hz frequency). A calibrated Silicon UV-enhanced photodiode was used as reference.

### Thin films characterization

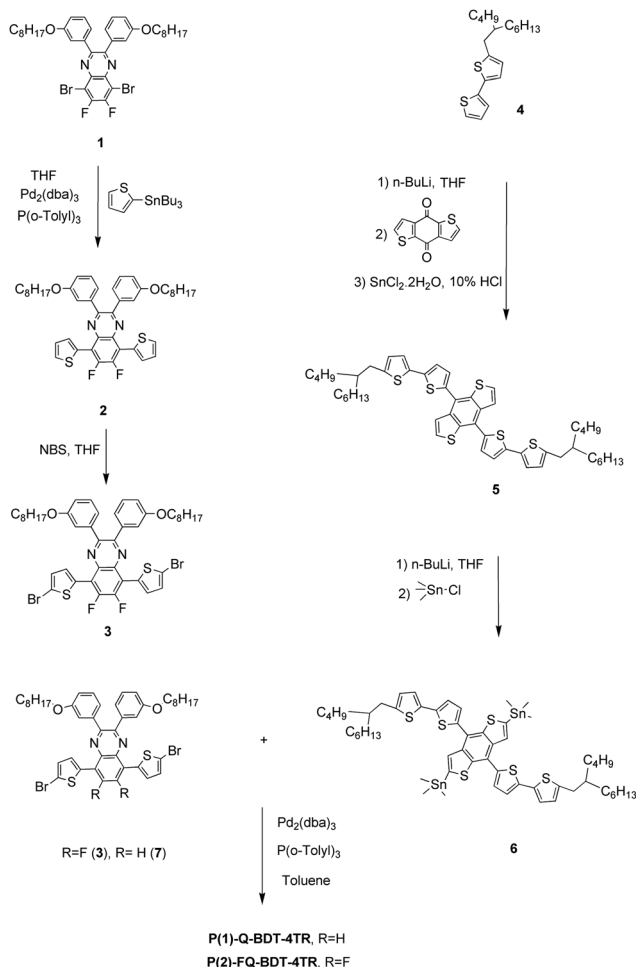
All thin-film characterizations were performed in air. Solution and thin film optical absorption spectra were recorded with a PerkinElmer Lambda 900 UV/Vis/NIR spectrophotometer. Atomic Force Microscopy (AFM) images were taken with a Solver Pro (NT-934 MDT) scanning probe microscope in tapping mode. The absorption spectra of blend films were recorded with a JASCO V-550 spectrophotometer. AFM images and blend films absorption spectra were recorded directly on the tested devices, in the device area out of the LiF/Al electrode. The hole mobility of the polymers in the active layers was measured through the space charge limited current (SCLC) method using devices with the structure ITO/PEDOT:PSS/polymer:PC<sub>61</sub>BM/Au.<sup>26</sup> The processing conditions used for the active layers were the optimized ones. Charge mobility was extracted by fitting the current density–voltage curves, recorded in dark conditions, to the Mott–Gurney equation:  $J = (9/8)(\mu\epsilon_r\epsilon_0V^2)d^{-3}$ , where *J* is the measured current density,  $\mu$  is the hole mobility,  $\epsilon_r$  is the relative permittivity of the active layer,  $\epsilon_0$  is the permittivity of vacuum, *d* is the thickness of the active layer and *V* is the applied voltage.

## Results and discussion

### Synthesis of monomers and polymers

Fig. 1 shows the structures of **P(1)-Q-BDT-4TR** and **P(2)-FQ-BDT-4TR** (abbreviated as **P(1)** and **P(2)**, respectively, in the text).

The routes towards the synthesis of the quinoxaline and BDT based monomers are illustrated in Scheme 1, while details are reported in the experimental section. Stille coupling reaction between 5,8-dibromo-6,7-difluoro-2,3-bis(3-(octyloxy)phenyl)quinoxaline (**1**), synthesized as previously reported,<sup>23</sup> and



**Scheme 1** Synthetic route for the preparation of monomers and of polymers **P(1)** and **P(2)**.

tributyl(thiophen-2-yl)stannane, gave compound **2** in excellent yield. Bromination of compound **2** with NBS in THF yielded the dibromo functionalized monomeric unit (**3**) which was used for the preparation of **P(2)-FQ-BDT-4TR** (or **P(2)**).<sup>17b</sup> The other quinoxaline based monomer (**7**) used for the synthesis of **P(1)-Q-BDT-4TR** (**P(1)**) was synthesized following a sequence of reactions previously reported.<sup>18b</sup> The BDT containing monomeric unit (**6**) was also prepared by two successive steps in high yield. 5-(2-Butyloctyl)-2,2'-bithiophene (**4**) was lithiated with  $n\text{-BuLi}$  and subsequently made to react with benzo[1,2-*b*:4,5-*b'*]dithiophene-4,8-dione. The material formed was reduced with  $\text{SnCl}_2 \cdot 2\text{H}_2\text{O}$  and 10% HCl *in situ* to give 4,8-bis(5'-(2-butyloctyl)-[2,2'-

bithiophen]-5-yl)benzo[1,2-*b*:4,5-*b'*]dithiophene (**5**). Finally, double lithiation of compound **5** followed by quenching with trimethyl tin chloride yielded the desired monomeric unit (**6**). The presence of four thiophene units as side chain made the BDT monomer to have a rigid and planar structure with strong tendency to crystallization. Hence the monomer was collected in its solid state, despite the presence of long and branched side chain, and it was possible to purify it by recrystallization from isopropanol. Polymers **P(1)** and **P(2)** were prepared *via* Stille coupling reaction of the corresponding quinoxaline based monomers with distannylated BDT monomer in toluene in the presence of  $\text{Pd}_2(\text{dba})_3/\text{P}(o\text{-Tolyl})_3$  as catalyst by heating at 90 °C under nitrogen atmosphere. The polymers were collected and purified following standard procedures (details are given in the Experimental section). The weight-average molecular weight ( $M_w$ ) and number-average molecular weight ( $M_n$ ) of the copolymers were determined by gel permeation chromatography (GPC) using polystyrene standards and TCB as an eluent. The  $M_w$  and  $M_n$  of **P(1)** resulted to be 47.4 and 16.3  $\text{kg mol}^{-1}$  and those of **P(2)** 46.1 and 18.5  $\text{kg mol}^{-1}$  respectively (Table 1). Since the two polymers present very similar molecular weight and polydispersity index, their properties and photovoltaic performances are discussed on the basis of their different chemical structure.

### Electrochemical and optical properties

The HOMO and LUMO energy levels of the two polymers, reported in Table 1, were calculated by square wave voltammetry (SWV) (Fig. S1 in ESI<sup>†</sup>), extrapolating them from the potentials of the first oxidation and reduction peaks registered.

The HOMO and LUMO energy levels of **P(1)** were estimated to lie at  $-5.68$  eV and  $-3.14$  eV respectively. In comparison, **P(2)** exhibits a deeper HOMO level at  $-5.96$  eV and a similar LUMO level lying at  $-3.20$  eV. The lowering of the HOMO of **P(2)** comparing to the HOMO of **P(1)** by 0.28 eV confirms the strong effect played by the electron withdrawing fluorine atoms.<sup>21a,27</sup> As expected, the influence of fluorine on the frontier orbital energies is more pronounced for the HOMO than for the LUMO, the latter differing only by 0.06 eV between the two polymers. Interestingly, the polymers **P(1)** and **P(2)** exhibit lower HOMO energy levels ( $-5.68$  and  $-5.96$  eV, respectively) with respect to the analogous PBDT-TFQ<sup>17b</sup> polymer based on alkoxy side chains, having HOMO and LUMO levels at  $-5.52$  and  $-3.30$  eV respectively. Even though a direct comparison between these values is not highly accurate for the different techniques used for their measurement (square wave and cyclic voltammetry respectively), **P(1)**- and **P(2)**-based devices could reasonably give

**Table 1** Summary of molecular weights, optical and electrochemical properties of **P(1)** and **P(2)**

Polymer	Solution <sup>b</sup>						Thin-film <sup>c</sup>					
	$M_n^a$ [kDa]	$M_w^a$ [kDa]	PDI	$\lambda_{\text{max}}$ [nm]	$\lambda_{\text{onset}}$ [nm]	$E_{\text{gap}}^{\text{opt,d}}$ [eV]	$\lambda_{\text{max}}$ [nm]	$\lambda_{\text{onset}}$ [nm]	$E_{\text{gap}}^{\text{opt,d}}$ [eV]	$E_{\text{HOMO}}$ [eV]	$E_{\text{LUMO}}$ [eV]	
<b>P(1)</b>	16.3	47.4	2.9	388, 597	700	2.07	388, 601, 636	720	1.73	-5.68	-3.14	
<b>P(2)</b>	18.5	46.1	2.5	390, 601	700	2.05	394, 606, 640	720	1.73	-5.96	-3.20	

<sup>a</sup> Determined by GPC. <sup>b</sup> In *o*-dichlorobenzene. <sup>c</sup> Spin-coated from *o*-dichlorobenzene solutions on glass substrates. <sup>d</sup>  $E_{\text{gap}}^{\text{opt}} = 1240/\lambda_{\text{onset}}$ .

devices with a higher  $V_{OC}$ , in agreement with the difference:  $HOMO_{donor} - LUMO_{acceptor}$ .<sup>28</sup> Moreover, the measured HOMO energies are in an ideal range to ensure good polymer air stability (being the oxidation threshold from air around  $-5.2$  eV).<sup>29</sup> In addition, considering that the LUMO level of the typical electron acceptors PC<sub>61</sub>BM and PC<sub>71</sub>BM are located at  $-4.03$  and  $-4.13$  eV respectively,<sup>30</sup> the offset between the excited state of the donor polymer and of the molecular acceptor should provide the driving force for an efficient exciton dissociation, ensuring energetically favorable electron transfer.

From the electrochemical data (EC), relatively high band gaps are extrapolated for the two polymers in solution: 2.54 eV and 2.76 eV respectively for **P(1)** and **P(2)** (Table 1). These values, despite a slight discrepancy likely dependent on the different methods employed, are consistent with those estimated from the absorption spectra in solution ( $E_{gap}^{opt}$ : 2.07 and 2.05 eV for **P(1)** and **P(2)**, respectively). However, the  $E_{gap}^{opt}$  estimated from the absorption spectra in solid state demonstrate how the polymer aggregation could determine an important decrease of the energy gap due to the effect of polymeric chains interactions. Indeed, the absorption onset value ( $\lambda_{onset}$ ) for **P(1)** and **P(2)** films is  $\sim 720$  nm, from which the resulting  $E_{gap}^{opt}$  are estimated to be  $\sim 1.73$  eV for both polymers.

The UV-visible absorption spectra of **P(1)** and **P(2)** in solution and in the solid state deposited as thin films on glass, with spectra normalized on the higher energy absorption band, are shown in Fig. 2. The two polymers show similar behavior both in solution and in thin film, with broad absorption spectra spanning from the UV region to above 700 nm. In diluted solution a first absorption band centered around 400 nm is observed for both polymers, attributable  $\pi-\pi^*$  transitions localized on the 2D  $\pi$ -conjugated units, as confirmed by the good overlap of this absorption band with the spectrum of the BDT monomeric precursor (**6**) in solution, also shown in Fig. 2. A lower energy absorption band, characteristic of the charge transfer (CT) state arising between the BDT and quinoxaline units, is then observed between 500 and 700 nm, with two relative maxima around 600 and 650 nm. In particular, an intramolecular CT state could be responsible for the peak

appearing at 600 nm, while the more red-shifted shoulder at 650 nm could be mainly due to inter-chain interactions.<sup>31</sup> The latter band then indicates the probable presence of molecular aggregates also in solution, confirming the good aggregation tendency of the polymers, promoted by their 2D highly  $\pi$ -conjugated structure. Note that the relative intensity of the CT band *versus* the  $\pi-\pi^*$  one is higher for **P(2)** than for **P(1)**, this indicating the stronger CT character of the former polymer comparing to the latter, due to the superior electron-withdrawing strength of the fluorine-substituted moiety comparing to the unsubstituted quinoxaline one.

Passing from solution to thin film absorption spectra, a red shift of the CT bands absorption maxima and onsets is registered for both **P(1)** and **P(2)**, accompanied by an intensity increase of the absorption shoulder at 650 nm relative to the shoulder around 600 nm. This indicates a high aggregation tendency of the two polymers in the solid state comparing to solution, in particular for **P(2)** comparing to **P(1)** probably due to its discussed stronger CT character.

It is interesting to note that both **P(1)** and **P(2)**, comparing to their analogous counterparts with alkoxy side chains P(BDT-DTQx)<sup>17a</sup> and PBDT-TFQ<sup>17b</sup> respectively, present a strong red shift (of 67 and 29 nm respectively) of the lower energy absorption maximum in thin film, confirming the role of the 2D  $\pi$ -conjugated side chains in promoting a high intermolecular  $\pi-\pi$  stack in the polymeric film.

A summary of the described optical properties of the two polymers, together with the electrochemical data, is shown in Table 1.

### Photovoltaic performance

The photovoltaic performance of **P(1)** and **P(2)** polymers was investigated by fabricating conventional BHJ solar cells having the following structure: ITO/PEDOT:PSS/active layer/LiF/Al. The active layers were prepared by spin-casting the polymer:PC<sub>61</sub>BM (or PC<sub>71</sub>BM) blends, with different (wt/wt) ratios, from *o*-dichlorobenzene (*o*-DCB) solutions. The photovoltaic parameters of the corresponding devices are shown in Table 2, while the  $J-V$  curves of optimized devices based on **P(1)** and **P(2)** with PC<sub>61</sub>BM or PC<sub>71</sub>BM are reported in Fig. 3.

Within the devices prepared with blends of **P(1)** and PC<sub>61</sub>BM in 1 : 2, 2 : 1 and 1 : 1 ratios, the device with an equal loading of polymer and fullerene shows a higher PCE, with the increase in PCE mainly originating from enhanced short-circuit current density ( $J_{SC}$ ). The best **P(1)**:PC<sub>61</sub>BM-based device shows a  $J_{SC}$  of  $-7.3$  mA cm<sup>-2</sup>, a  $V_{OC}$  of 0.74 V and a FF of 58%, resulting in an overall PCE of 3.2% (Fig. 3a and Table 2). For all **P(1)** : PC<sub>61</sub>BM donor : acceptor ratios, the effect of thermal annealing is to enhance the device  $J_{SC}$  and FF while only slightly decreasing the  $V_{OC}$  (by  $\sim 30-40$  mV), indicating a probable reordering of the polymer chains into a morphology which facilitates charge separation, transport and improves the overall device efficiency.<sup>32</sup> Even a higher performance is obtained for the **P(1)**:PC<sub>71</sub>BM-based device with annealed active layer in 1 : 1 polymer:fullerene blend ratio, which shows enhanced  $J_{SC}$  ( $-9.5$  mA cm<sup>-2</sup>) and consequently higher PCE (3.7%) comparing to

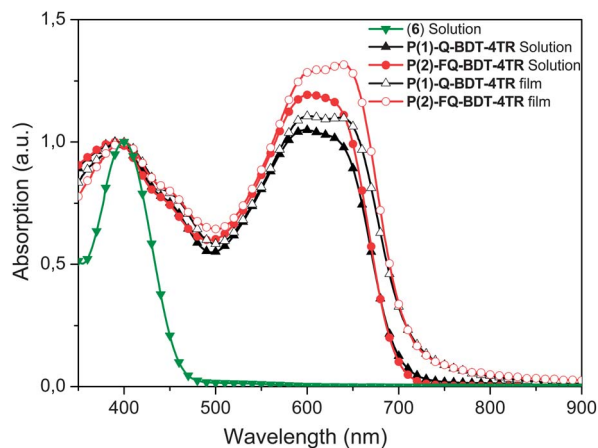


**Fig. 2** Optical absorption of monomer **6** in CHCl<sub>3</sub> solution and of polymers **P(1)** and **P(2)** in solid state and in *o*-dichlorobenzene solution.

**Table 2** Summary of photovoltaic parameters of the device based on **P(1)** or **P(2)** and PC<sub>61</sub>BM or PC<sub>71</sub>BM blends, in different polymer : fullerene ratios and annealing conditions. Values were averaged over 6 devices each. For optimized devices, the maximum values are reported in brackets

Polymer : PC <sub>xx</sub> BM ratio (wt/wt)	T <sub>ANN.</sub> [°C]	V <sub>OC</sub> [V]	J <sub>SC</sub> [mA cm <sup>-2</sup> ]	FF [%]	PCE [%]
<b>P(1)</b> : PC <sub>61</sub> BM (1 : 2)	—	0.70	-5.8	42	1.7
<b>P(1)</b> : PC <sub>61</sub> BM (1 : 2)	110/5'	0.73	-6.3	61	2.8
<b>P(1)</b> : PC <sub>61</sub> BM (1 : 1)	—	0.78	-6.5	34	1.7
<b>P(1)</b> : PC <sub>61</sub> BM (1 : 1)	110/5'	0.74	-7.3	58	3.2
<b>P(1)</b> : PC <sub>61</sub> BM (2 : 1)	—	0.80	-3.6	28	0.8
<b>P(1)</b> : PC <sub>61</sub> BM (2 : 1)	110/5'	0.75	-6.0	35	1.6
<b>P(1)</b> : PC <sub>71</sub> BM (1 : 1)	—	0.77	-7.1	48	2.6
<b>P(1)</b> : PC <sub>71</sub> BM (1 : 1)	110/5'	0.74	-9.5	53	3.7
<b>P(2)</b> : PC <sub>61</sub> BM (1 : 2)	—	0.87	-7.9	56	3.8
<b>P(2)</b> : PC <sub>61</sub> BM (1 : 2)	110/5'	0.86	-6.1	65	3.4
<b>P(2)</b> : PC <sub>61</sub> BM (1 : 1)	—	0.90	-10.2	58	5.3 (5.5)
<b>P(2)</b> : PC <sub>61</sub> BM (1 : 1)	110/5'	0.86	-9.4	65	5.2 (5.3)
<b>P(2)</b> : PC <sub>61</sub> BM (2 : 1)	—	0.91	-6.9	33	2.1
<b>P(2)</b> : PC <sub>61</sub> BM (2 : 1)	110/5'	0.89	-8.7	41	3.1
<b>P(2)</b> : PC <sub>71</sub> BM (1 : 1)	—	0.90	-9.3	57	4.7
<b>P(2)</b> : PC <sub>71</sub> BM (1 : 1)	110/5'	0.88	-8.7	60	4.5

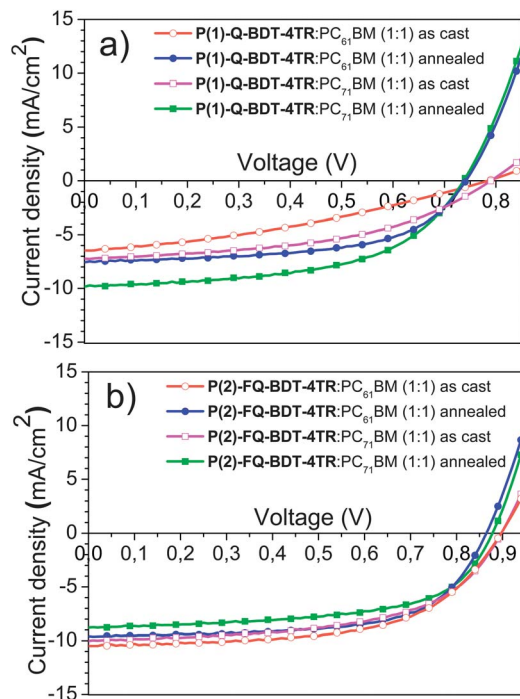


**Fig. 3** *J*-*V* curves of the most representative devices based on: (a) **P(1)** and (b) **P(2)**.

the **P(1)**:PC<sub>61</sub>BM-based device (Fig. 3a and Table 2), thanks to the contribution of PC<sub>71</sub>BM to light absorption in the visible region and hence to charge carrier generation.<sup>33</sup> Note that the optimized **P(1)**:PC<sub>71</sub>BM-based device, compared to the one based on the analogous polymer with alkoxy side chains instead of 2D  $\pi$ -conjugated ones<sup>17a</sup> (**P**(BDT-DTQx):PC<sub>71</sub>BM-based device), presents a doubled *J*<sub>SC</sub> (-9.5 versus -4.9 mA cm<sup>-2</sup>) and a higher *V*<sub>OC</sub> (0.74 versus 0.65 V).

This confirms the positive effect of the 2D  $\pi$ -conjugated side-chains (comparing to alkoxy-side chains), which effectively

leads to: (i) red-shifted absorption spectrum with enhanced interchain  $\pi$ - $\pi$  interactions, that correlates well with the improved *J*<sub>SC</sub>; (ii) lower polymer HOMO energy, in agreement with the larger device *V*<sub>OC</sub>.

Devices based on the fluorinated polymer **P(2)** in general show an improved photovoltaic performance with respect to **P(1)** (Fig. 3b and Table 2). By comparing the devices prepared with the two different polymers in analogous conditions, an increase in *V*<sub>OC</sub> by 0.13 V on average is observed passing from **P(1)** to **P(2)**, due to the discussed effect of the F atoms in lowering the polymer HOMO level (Table 1).<sup>32,34</sup> The best performance is obtained for the devices based on as-cast **P(2)**:PC<sub>61</sub>BM blend with a polymer : fullerene ratio of 1 : 1 (wt/wt), showing on average a *J*<sub>SC</sub> of -10.2 mA cm<sup>-2</sup>, a *V*<sub>OC</sub> of 0.90 V, a FF of 58% and a PCE of 5.3% (5.5% for the best device). It has to be emphasized that the synergic effect of the fluorine atom and of the 2D  $\pi$ -conjugated side chains in **P(2)** allows to obtain a higher *V*<sub>OC</sub> (0.90 V in the best performing device) with respect to the analogous polymer with alkoxy-side chains (**P**(BDT-TFQ):PC<sub>61</sub>BM one is observed (5.3% and 6.9% respectively). This could be explained on the basis of some differences, other than the substitution on the BDT core, such as: the different length of the alkoxy side chains on the quinoxaline unit (octyl and hexyl respectively) and the different cathode buffer layers employed in the devices (LiF and Ca, respectively).

By comparing the photovoltaic performance of **P(2)**:PC<sub>61</sub>BM-based devices with that of the analogous optimized **P(1)**:PC<sub>61</sub>BM-based ones, the higher efficiency in the former case can be ascribed, other than to the higher *V*<sub>OC</sub>, to enhanced *J*<sub>SC</sub> and FF. This could be due to the effect of the F atoms in favoring the  $\pi$ - $\pi$  polymer chains interactions, already promoted by the high 2D  $\pi$ -conjugation, which enhances the polymer light absorption and most importantly its charge carrier mobility.<sup>21a</sup> Indeed, the hole mobility of the **P(2)**:PC<sub>61</sub>BM optimized blend

resulted to be three times higher with respect to the mobility of the optimized **P(1)**:PC<sub>61</sub>BM blend ( $2.4 \times 10^{-4} \text{ cm}^2 \text{ V}^{-1} \cdot \text{s}^{-1}$  and  $0.8 \times 10^{-4} \text{ cm}^2 \text{ V}^{-1} \cdot \text{s}^{-1}$  respectively, Fig. S19 and S18 in ESI†). Moreover, the strong  $\pi$ - $\pi$  intermolecular interactions of **P(2)** allow the achievement of a **P(2)**:PC<sub>61</sub>BM blend film with a morphology giving optimized photovoltaic performances without the need for additional thermal treatment.

A lower performance is obtained for the optimized **P(2)**:PC<sub>71</sub>BM-based device (Fig. 3b and Table 2), probably due to a lower miscibility of the polymer with PC<sub>71</sub>BM leading to a less favorable morphology of the **P(2)**:PC<sub>71</sub>BM film comparing to the analogous PC<sub>61</sub>BM-based film. However, the optimized **P(2)**:PC<sub>71</sub>BM based devices showed an efficiency of 4.7%, with a  $J_{\text{SC}}$  of  $-9.3 \text{ mA cm}^{-2}$ , a  $V_{\text{OC}}$  of 0.90 V and a FF of 57%.

The EQE spectra of the best polymer:PC<sub>61</sub>BM based devices, as shown in Fig. 4a, have similar spectral features of the corresponding blends absorption spectra (Fig. 4b), with higher values for the **P(2)**-based blend comparing to the **P(1)**-based one (0.52 and 0.43 on the maximum respectively, corresponding to the relative polymers absorption maxima). Convolution of these EQE spectra with the 1.5AM solar spectrum give calculated short circuit current densities in good agreement, within a  $\sim 10\%$  experimental error, with those obtained from  $J$ - $V$  measurements.

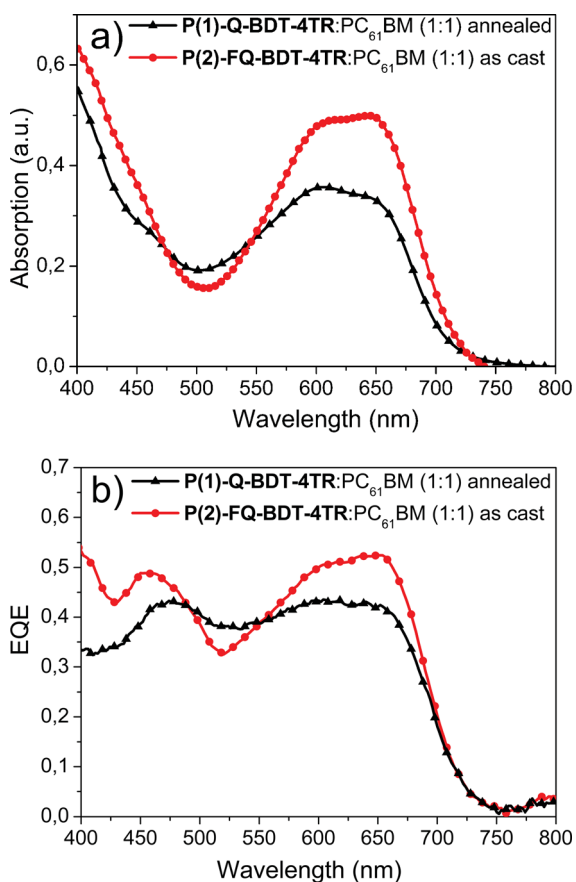


**Fig. 4** Normalized absorption spectra (a) and EQE spectra (b) of optimized devices based on annealed (1 : 1) **P(1)**:PC<sub>61</sub>BM (black line) and as-cast (1 : 1) **P(2)**:PC<sub>61</sub>BM films (red line).

## Morphological analysis

Morphological analysis were done on annealed and as-cast polymer:PC<sub>61</sub>BM films in 1 : 1 ratio (optimized blend ratio) to have a deeper insight on the different effect of annealing on the morphology of the two polymers-based blends and on the corresponding device performances. By comparing **P(1)**:PC<sub>61</sub>BM as-cast and annealed films, similar film roughness of  $\sim 1 \text{ nm}$  (calculated as Root Mean Square deviation, or RMS) are registered, even though the **P(1)**:PC<sub>61</sub>BM annealed film (Fig. 5b) exhibits a superficial morphology with slightly reduced domain size and finer nanostructures comparing to as-cast film (Fig. 5a). On the opposite, an evident increase in roughness is found when passing from **P(2)**:PC<sub>61</sub>BM as cast film to the annealed one, with RMS going from  $\sim 1 \text{ nm}$  to  $\sim 3 \text{ nm}$ . Note that for **P(2)**:PC<sub>61</sub>BM blends the annealed film (Fig. 5d) exhibits a less structured surface with relatively larger domains comparing to the analogous as-cast film (Fig. 5c), being this an opposite trend in the film nanostructuring with heat comparing to **P(1)**-based blends.

As a result, thermal annealing leads to an increase in  $J_{\text{SC}}$  and in FF for the **P(1)**:PC<sub>61</sub>BM-based devices, while for **P(2)**-based devices annealing causes a decrease in  $J_{\text{SC}}$  and a modest increase in FF (Table 2). This is most probably due to a better packaging/ordering of the **P(1)** polymer chains induced by annealing, in agreement with the finer reorganization of the active layer surface despite the identical surface roughness, which improves the polymer electrical and optical properties. On the other hand, the stronger interchain interactions of **P(2)** comparing to **P(1)**, due to the presence of the F atoms in the polymer backbone and to its discussed stronger CT character, leads to a more defined and finer polymer self-organization in as-cast blend films (Fig. 5c). As a consequence, since the effect of annealing on the **P(2)**:PC<sub>61</sub>BM blend is probably to induce further aggregation, an increase of the polymer domains sizes

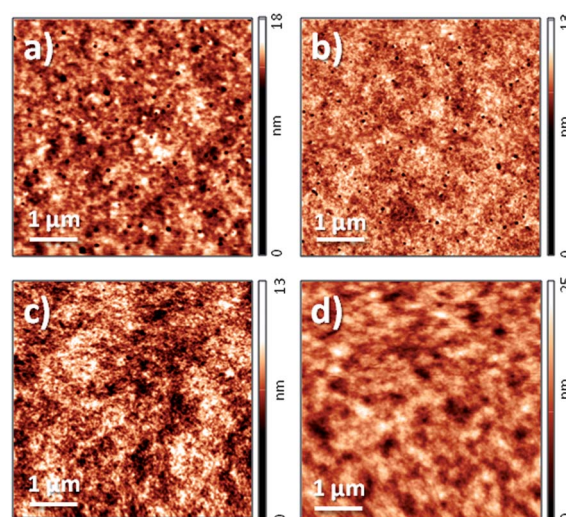


**Fig. 5** AFM images (size:  $5 \times 5 \mu\text{m}$ ) of blend films on ITO/PEDOT:PSS of: (a) **P(1)**:PC<sub>61</sub>BM (1 : 1) as cast, RMS = 0.8 nm; (b) **P(1)**:PC<sub>61</sub>BM (1 : 1) annealed, RMS = 0.9 nm; (c) **P(2)**:PC<sub>61</sub>BM (1 : 1) as cast, RMS = 1.3 nm; (d) **P(2)**:PC<sub>61</sub>BM (1 : 1) annealed, RMS = 3.4 nm.

and a higher separation of the fullerene and polymer phases with a lower D–A interfacial area probably occurs, decreasing the corresponding annealed device  $J_{SC}$  and efficiency.

## Conclusions

In conclusion, we synthesized and characterized two donor-acceptor alternating polymers based on quinoxaline and BDT comonomers. Both polymers have a highly 2D  $\pi$ -conjugated structure obtained through the insertion of thiophene-conjugated side chains on the BDT unit, leading to red-shifted absorption spectra, improved thermal stability and lower HOMO energies comparing to the analogous alkyl-substituted copolymers. Moreover, the substitution of fluorine atoms on the quinoxaline moiety in one of the two polymers was demonstrated to improve the resulting thin film optical, electrical and morphological properties by inducing a further lowering of its HOMO energy level and by promoting intermolecular  $\pi$ – $\pi$  interactions. Electrochemical measurements, UV-visible absorption spectra and morphological studies were carried out to get insights on the differences between the two synthesized materials. BHJ solar cells prepared in different conditions of polymer:fullerene blend ratio, thermal treatment and acceptor nature allowed the gradual optimization of the photovoltaic performances, other than allowing to evidence the two polymers optical, electrical and physical properties. As a result of the cooperative effect of the fluorine atoms and alkyl-dithiophene side substitution, the best performing solar cells, using PC<sub>61</sub>BM as acceptor, showed a PCE of 5.3% (5.5% for the best device) with  $J_{SC}$ , FF and  $V_{OC}$  of  $-10.2 \text{ mA cm}^{-2}$ , 58% and 0.90 V, respectively, without the need for additional solvent additive or thermal treatments. This work emphasizes the effectiveness of using highly 2D  $\pi$ -conjugated units and highly electron withdrawing side substituents for the design of efficient active donor materials having broader absorption spectra, high photocurrents and  $V_{OC}$  when employed in BHJ organic solar cells.

## Acknowledgements

This work was financially supported by the European Commission FP7 collaborative project SUNFLOWER (FP7-ICT-2011-7, Grant no. 287594), by Programma Operativo FESR 2007–2013 of Regione Emilia-Romagna – Attività I.1.1 and by Progetto Premiale CNR 2012 – Produzione di energia da fonti rinnovabili (Iniziativa CNR per il Mezzogiorno, L. 191/2009 art. 2 comma 44). We also acknowledge Chalmers' Area of Advance Materials Science for funding. EW acknowledges the Swedish Research Council for financial support.

## Notes and references

- (a) G. Li, R. Zhu and Y. Yang, *Nat. Photonics*, 2012, **6**, 153; (b) F. C. Krebs, *Sol. Energy Mater. Sol. Cells*, 2009, **93**, 394; (c) R. R. Søndergaard, M. Hösel and F. C. Krebs, *J. Polym. Sci., Part B: Polym. Phys.*, 2013, **51**, 16.
- (a) L. Dou, J. You, J. Yang, C.-C. Chen, Y. He, S. Murase, T. Moriarty, K. Emery, G. Li and Y. Yang, *Nat. Photonics*, 2012, **6**, 180; (b) Y.-J. Cheng, S.-H. Yang and C.-S. Hsu, *Chem. Rev.*, 2009, **109**, 5868; (c) Y. Li, *Acc. Chem. Res.*, 2012, **45**, 723; (d) M. C. Scharber, D. Mühlbacher, M. Koppe, P. Denk, C. Waldauf, A. J. Heeger and C. J. Brabec, *Adv. Mater.*, 2006, **18**, 789; (e) S. H. Park, A. Roy, S. Beaupré, S. Cho, N. Coates, J. S. Moon, D. Moses, M. Leclerc, K. Lee and A. J. Heeger, *Nat. Photonics*, 2009, **3**, 297; (f) J. Yuan, Z. Zhai, H. Dong, J. Li, Z. Jiang, Y. Li and W. Ma, *Adv. Funct. Mater.*, 2013, **23**, 885.
- (a) D. Jarzab, F. Cordella, M. Lenes, F. B. Kooistra, P. W. M. Blom, J. C. Hummelen and M. A. Loi, *J. Phys. Chem. B*, 2009, **113**, 16513; (b) N. D. Treat, L. M. Campos, M. D. Dimitriou, B. Ma, M. L. Chabinye and C. J. Hawker, *Adv. Mater.*, 2010, **22**, 4982; (c) P. E. Keivanidis, V. Kamm, C. Dyer-Smith, W. Zhang, F. Laquai, I. McCulloch, D. D. C. Bradley and J. Nelson, *Adv. Mater.*, 2010, **22**, 5183; (d) A. W. Hains, C. Ramanan, M. D. Irwin, J. Liu, M. R. Wasielewski and T. J. Marks, *ACS Appl. Mater. Interfaces*, 2010, **2**, 175; (e) A. W. Hains, J. Liu, A. B. F. Martinson, M. D. Irwin and T. J. Marks, *Adv. Funct. Mater.*, 2010, **20**, 595; (f) M. D. Irwin, J. D. Servaites, D. B. Buchholz, B. J. Leever, J. Liu, J. D. Emery, M. Zhang, J.-H. Song, M. F. Durstock, A. J. Freeman, M. J. Bedzyk, M. C. Hersam, R. P. H. Chang, M. A. Ratner and T. J. Marks, *Chem. Mater.*, 2011, **23**, 2218; (g) M. Graetzel, R. A. J. Janssen, D. B. Mitzi and E. H. Sargent, *Nature*, 2012, **488**, 304; (h) E. L. Ratcliff, A. Garcia, S. A. Paniagua, S. R. Cowan, A. J. Giordano, D. S. Ginley, S. R. Marder, J. J. Berry and D. C. Olson, *Adv. Energy Mater.*, 2013, **3**, 647; (i) M. Bolognesi, M. Tassarolo, T. Posati, M. Nocchetti, V. Benfenati, M. Seri, G. Ruani and M. Muccini, *Organic Photonics and Photovoltaics*, 2013, **1**, 1; (j) M. Bolognesi, A. Sanchez-Diaz, J. Ajuria, R. Pacios and E. Palomares, *Phys. Chem. Chem. Phys.*, 2011, **13**, 6105.
- (a) S. Fabiano, Z. Chen, S. Vahedi, A. Facchetti, B. Pignataro and M. A. Loi, *J. Mater. Chem.*, 2011, **21**, 5891; (b) S. Yamamoto, A. Orimo, H. Ohkita, H. Benten and S. Ito, *Adv. Energy Mater.*, 2012, **2**, 229; (c) R. A. J. Janssen and J. Nelson, *Adv. Mater.*, 2013, **25**, 1847.
- (a) Z. He, C. Zhong, S. Su, M. Xu, H. Wu and Y. Cao, *Nat. Photonics*, 2012, **6**, 591; (b) J. You, L. Dou, K. Yoshimura, T. Kato, K. Ohya, T. Moriarty, K. Emery, C.-C. Chen, J. Gao, G. Li and Y. Yang, *Nat Commun.*, 2013, **4**, 1446.
- <http://www.polyera.com/newsflash/polyera-achieves-world-record-organic-solar-cell-performance>.
- (a) G. Dennler, M. C. Scharber and C. J. Brabec, *Adv. Mater.*, 2009, **21**, 1323; (b) M. Seri, A. Marrocchi, D. Bagnis, R. Ponce, A. Taticchi, T. J. Marks and A. Facchetti, *Adv. Mater.*, 2011, **23**, 3827.
- (a) B. C. Thompson and J. M. J. Frechet, *Angew. Chem., Int. Ed.*, 2008, **47**, 58; (b) S. Günes, H. Neugebauer and N. S. Sariciftci, *Chem. Rev.*, 2007, **107**, 1324; (c) G. Li, V. Shrotriya, Y. Yao, J. S. Huang and Y. Yang, *J. Mater. Chem.*, 2007, **17**, 3126.
- (a) M. C. Scharber, D. Mühlbacher, M. Koppe, P. Denk, C. Waldauf, A. J. Heeger and C. J. Brabec, *Adv. Mater.*, 2006, **18**, 789; (b) Y. Li, *Chem.-Asian J.*, 2013, **8**, 2316.

- 10 M. Jørgensen, K. Norrman, S. A. Gevorgyan, T. Tromholt, B. Andreasen and F. C. Krebs, *Adv. Mater.*, 2012, **24**, 580.
- 11 (a) P. W. M. Blom, V. D. Mihailetschi, L. J. A. Koster and D. E. Markov, *Adv. Mater.*, 2007, **19**, 1551; (b) H. Hoppe and N. S. Sariciftci, *J. Mater. Res.*, 2004, **19**, 1924; (c) B. Kippelen and J.-L. Bredas, *Energy Environ. Sci.*, 2009, **2**, 251; (d) H. Hoppe and N. S. Sariciftci, *Adv. Polym. Sci.*, 2008, **214**, 1.
- 12 (a) H. J. Son, F. He, B. Carsten and L. Yu, *J. Mater. Chem.*, 2011, **21**, 18934; (b) Y.-J. Cheng, S.-H. Yang and C.-S. Hsu, *Chem. Rev.*, 2009, **109**, 5868; (c) A. Facchetti, *Chem. Mater.*, 2011, **23**, 733; (d) Y. Li, *Acc. Chem. Res.*, 2012, **45**, 723; (e) H. J. Son, B. Carsten, I. H. Jung and L. Yu, *Energy Environ. Sci.*, 2012, **5**, 8158; (f) A. Abbotto, E. Herrera Calderon, M. S. Dangate, F. De Angelis, N. Manfredi, C. M. Mari, C. Marinzi, E. Mosconi, M. Muccini, R. Ruffo and M. Seri, *Macromolecules*, 2010, **43**, 9698; (g) A. Abbotto, M. Seri, M. S. Dangate, F. De Angelis, N. Manfredi, E. Mosconi, M. Bolognesi, R. Ruffo, M. M. Salamone and M. Muccini, *J. Polym. Sci., Part A: Polym. Chem.*, 2012, **50**, 2829; (h) S. Lu, M. Drees, Y. Yao, D. Boudinet, H. Yan, H. Pan, J. Wang, Y. Li, H. Usta and A. Facchetti, *Macromolecules*, 2013, **46**, 3895.
- 13 (a) C. Duan, F. Huang and Y. Cao, *J. Mater. Chem.*, 2012, **22**, 10416; (b) M. Chen, E. Perzon, M. R. Andersson, S. Marcinkevicius, S. K. M. Jonsson, M. Fahlman and M. Berggren, *Appl. Phys. Lett.*, 2004, **84**, 3570; (c) C. Kitamura, S. Tanaka and Y. Yamashita, *Chem. Mater.*, 1996, **8**, 570; (d) Y. Liang, Z. Xu, J. Xia, S.-T. Tsai, Y. Wu, G. Li, C. Ray and L. Yu, *Adv. Mater.*, 2010, **22**, E135–E138; (e) T.-Y. Chu, J. Lu, S. Beaupré, Y. Zhang, J.-R. Pouliot, S. Wakim, J. Zhou, M. Leclerc, Z. Li, J. Ding and Y. Tao, *J. Am. Chem. Soc.*, 2011, **133**, 4250.
- 14 S. A. Jenekhe, L. Lu and M. M. Alam, *Macromolecules*, 2001, **34**, 7315.
- 15 (a) L. Bürgi, M. Turbiez, R. Pfeiffer, F. Bienewald, H. Kirner and C. Winnewisser, *Adv. Mater.*, 2008, **20**, 2217; (b) Y. Li, S. P. Singh and P. Sonar, *Adv. Mater.*, 2010, **22**, 4862; (c) H. N. Tsao, D. M. Cho, I. Park, M. R. Hansen, A. Mavrinskiy, D. Y. Yoon, R. Graf, W. Pisula, H. Spiess and K. Müllen, *J. Am. Chem. Soc.*, 2011, **133**, 2605.
- 16 E. Zhou, J. Cong, K. Tajima and K. Hashimoto, *Chem. Mater.*, 2010, **22**, 4890.
- 17 (a) Y. Fu, H. Cha, S. Song, G.-Y. Lee, C. E. Park and T. Park, *J. Polym. Sci., Part A: Polym. Chem.*, 2013, **51**, 372; (b) H.-C. Chen, Y.-H. Chen, C.-C. Liu, Y.-C. Chien, S.-W. Chou and P.-T. Chou, *Chem. Mater.*, 2012, **24**, 4766.
- 18 (a) A. Gadisa, W. Mammo, L. M. Andersson, S. Admassie, F. Zhang, M. R. Andersson and O. Inganäs, *Adv. Funct. Mater.*, 2007, **17**, 3836; (b) D. Gedefaw, Y. Zhou, S. Hellström, L. Lindgren, L. M. Andersson, F. Zhang, W. Mammo, O. Inganäs and M. R. Andersson, *J. Mater. Chem.*, 2009, **19**, 5359.
- 19 R. Duan, L. Ye, X. Guo, Y. Huang, P. Wang, S. Zhang, J. Zhang, L. Huo and J. Hou, *Macromolecules*, 2012, **45**, 3032.
- 20 (a) Y. Lu, Z. Xiao, Y. Yuan, H. Wu, Z. An, Y. Hou, C. Gao and J. Huang, *J. Mater. Chem. C*, 2013, **1**, 630.
- 21 (a) S. C. Price, A. C. Stuart, L. Yang, H. Zhou and W. You, *J. Am. Chem. Soc.*, 2011, **133**, 4625; (b) Y. Zhang, L. Gao, C. He, Q. Sun and Y. Li, *Polym. Chem.*, 2013, **4**, 1474.
- 22 (a) J. Min, Z.-G. Zhang, S. Zhang and Y. Li, *Chem. Mater.*, 2012, **24**, 3247; (b) J. Hou, Z. Tan, Y. Yan, Y. He, C. Yang and Y. Li, *J. Am. Chem. Soc.*, 2006, **128**, 4911; (c) Y. Li and Y. Zou, *Adv. Mater.*, 2008, **20**, 2952; (d) L. Huo, S. Zhang, X. Guo, F. Xu, Y. Li and J. Hou, *Angew. Chem., Int. Ed.*, 2011, **50**, 9697; (e) Y. Huang, X. Guo, F. Liu, L. Huo, Y. Chen, T. P. Russell, C. C. Han, Y. Li and J. Hou, *Adv. Mater.*, 2012, **24**, 3383; (f) F. Zhang, V. Roznyatovskiy, F.-R. F. Fan, V. Lynch, J. L. Sessler and A. J. Bard, *J. Phys. Chem. C*, 2011, **115**(5), 2592.
- 23 R. Kroon, R. Gehlhaar, T. T. Steckler, P. Henriksson, C. Mulur, J. Bergqvist, A. Hadipour, P. Heremans and M. R. Andersson, *Sol. Energy Mater. Sol. Cells*, 2012, **105**, 280.
- 24 V. V. Pavlishchuk and A. W. Addison, *Inorg. Chim. Acta*, 2000, **298**, 97.
- 25 A. J. Bard and L. R. Faulkner, *Electrochemical methods: fundamentals and applications*, Wiley, New York, 2001.
- 26 (a) N. Zhou, X. Guo, R. Ponce Ortiz, S. Li, S. Zhang, R. P. H. Chang, A. Facchetti and T. J. Marks, *Adv. Mater.*, 2012, **24**, 2242; (b) A. Abbotto, E. Herrera Calderon, M. S. Dangate, F. De Angelis, N. Manfredi, C. M. Mari, C. Marinzi, E. Mosconi, M. Muccini, R. Ruffo and M. Seri, *Macromolecules*, 2010, **43**, 9698; (c) D. S. Chung, D. H. Lee, C. Yang, K. Hong, C. E. Park, J. W. Park and S. K. Kwon, *Appl. Phys. Lett.*, 2008, **93**, 033303; (d) P. W. M. Blom, M. J. M. De Jong and J. J. M. Vleggaar, *Appl. Phys. Lett.*, 1996, **68**, 3308.
- 27 (a) H. J. Son, W. Wang, T. Xu, Y. Liang, Y. Wu, G. Li and L. Yu, *J. Am. Chem. Soc.*, 2011, **133**, 1885; (b) H.-Y. Chen, J. Hou, S. Zhang, Y. Liang, G. Yang, Y. Yang, L. Yu, Y. Wu and G. Li, *Nat. Photonics*, 2009, **3**, 649; (c) H. Zhou, L. Yang, A. C. Stuart, S. C. Price, S. Liu and W. You, *Angew. Chem., Int. Ed.*, 2011, **50**, 2995; (d) K. Reichenbacher, H. I. Süss and J. Hulliger, *Chem. Soc. Rev.*, 2005, **34**, 22; (e) M. Pagliaro and R. Ciriminna, *J. Mater. Chem.*, 2005, **15**, 4981.
- 28 C. J. Brabec, A. Cravino, D. Meissner, N. S. Sariciftci, T. Fromherz, M. T. Rispens, L. Sanchez and J. C. Hummelen, *Adv. Funct. Mater.*, 2001, **11**, 374.
- 29 (a) Y. Li, Q. Guo, Z. Li, J. Pei and W. Tian, *Energy Environ. Sci.*, 2010, **3**, 1427; (b) S. Beaupré, M. Belletête, G. Durocher and M. Leclerc, *Macromol. Theory Simul.*, 2011, **20**, 13; (c) D. M. de Leeuw, M. M. J. Simenon, A. R. Brown and R. E. F. Einerhand, *Synth. Met.*, 1997, **87**, 53.
- 30 E. Wang, L. Hou, Z. Wang, S. Hellström, W. Mammo, F. Zhang, O. Inganäs and M. R. Andersson, *Org. Lett.*, 2010, **12**, 4470.
- 31 M.-C. Yuan, M.-Y. Chiu, C.-M. Chiang and K.-H. Wei, *Macromolecules*, 2010, **43**, 6270.
- 32 C.-P. Chen, Y.-C. Chen and C.-Y. Yu, *Polym. Chem.*, 2013, **4**, 1161.
- 33 M. M. Wienk, J. M. Kroon, W. J. H. Verhees, J. Knol, J. C. Hummelen, P. A. van Hal and R. A. J. Janssen, *Angew. Chem., Int. Ed.*, 2003, **42**, 3371.
- 34 C. J. Brabec, A. Cravino, D. Meissner, N. S. Sariciftci, T. Fromherz, M. T. Rispens, L. Sanchez and J. C. Hummelen, *Adv. Funct. Mater.*, 2001, **11**, 374.